PNAS RESEARCH ARTICLE | NEUROSCIENCE

Coexistence within one cell of microvillous and ciliary phototransductions across M1- through M6-IpRGCs

Guang Li[a,1], Lujing Chen[a,b,2], Zheng Jiang[a,3], and King-Wai Yau[a,1]

Contributed by King-Wai Yau; received September 2, 2023; accepted November 16, 2023; reviewed by Robert J. Lucas and Akihisa Terakita

Intrinsically photosensitive retinal ganglion cells (ipRGCs) serve as primary photoceptors by expressing the photopigment, melanopsin, and also as retinal relay neurons for rod and cone signals en route to the brain, in both cases for the purpose of non-image vision as well as aspects of image vision. So far, six subtypes of ipRGCs (M1 through M6) have been characterized. Regarding their phototransduction mechanisms, we have previously found that, unconventionally, rhabdomeric (microvillous) and ciliary signaling motifs co-exist within a given M1-, M2-, and M4-ipRGC, with the first mechanism involving PLCβ4 and TRPC6,7 channels and the second involving cAMP and HCN channels. We have now examined M3-, M5-, and M6-cells and found that each cell likewise uses both signaling pathways for phototransduction, despite differences in the percentage representation by each pathway in a given ipRGC subtype for bright-flash responses (and saturated except for M6-cells). Generally, M3- and M5-cells show responses quite similar in kinetics to M2-responses, and M6-cell responses resemble broadly those of M1-cells although much lower in absolute sensitivity and amplitude. Therefore, similar to rod and cone subtypes in image vision, ipRGC subtypes possess the same phototransduction mechanism(s) even though they do not show microvilli or cilia morphologically.

ipRGC subtypes | uniform phototransduction mechanism | cross-motif GPCR signaling | G_q | cAMP

Significance

Intrinsically photosensitive retinal ganglion cells (ipRGCs) were discovered relatively recently. They mediate non-image and partly image vision and are currently divided into six subtypes (M1 through M6) based on their dendritic morphology and arborization locations. Previously, we found that M1-, M2-, and M4-ipRGCs have two co-existent phototransduction mechanisms within a given cell, one involving phospholipase C beta 4 (PLCβ4) and canonical transient receptor potential 6 and 7 (TRPC6,7) channels (microvillous motif) and the other involving cyclic Adenosine Monophosphate (cAMP) and hyperpolarization-activated cyclic nucleotide-gated (HCN) channels (ciliary motif). We now found the same in M3-, M5-, and M6-ipRGCs, although different percentage representations by the two mechanisms are present broadly across the six subtypes for bright-flash responses.

In mammals, retinal rods and cones serve as the primary photoreceptors for providing visual images of the ambience together with their dynamic details such as motion, direction of movement, color, etc. (image-forming vision). Separately, a special population of retinal ganglion cells (RGCs), which comprises third-order retinal neurons, exists that express the visual pigment, melanopsin, and therefore are also primary photoreceptors (1–11). They are called intrinsically photosensitive RGCs (ipRGCs) and serve non-image-forming vision such as photoentrainment of circadian rhythm, pupillary light reflex, and other subconscious bodily responses to ambient light, as well as image vision such as contrast sensitivity and color opponency by relaying at least signals from the retinal rod/cone pathways to a variety of brain nuclei (4–10).

Based on their dendritic morphology and arborization locations in the retinal inner plexiform layer, six subtypes of ipRGCs have so far been identified, M1 through M6 (6–11). These subtypes differ also in their absolute light sensitivity, pigment density, saturated response amplitude, as well as axonal targets in the brain. In terms of phototransduction mechanism, two have so far been recognized. One has a rhabdomeric (microvillous) motif (12–14), which we and others first characterized in M1-cells as follows: photoexcited melanopsin → $G\alpha_{q,11,14}$*(i.e., significant redundancy in downstream Gα's, where "*" indicates the active state, with GTP bound to Gα) → PLCβ4* → open TRPC6,7 channels (i.e., heteromeric TRPC channels comprising isoforms 6 and 7) → membrane depolarization → action-potential firing (15–18). This pathway is referred to here as the PLCβ4/TRPC6,7 pathway (16–18). It is essentially identical to that found in the rhabdomeric photoreceptors of the *Drosophila* eye, with $G\alpha_{q,11,14}$ being the multiple vertebrate homologs (which include also $G\alpha_{15}$, although $G\alpha_{15}$ is apparently not involved in the function under discussion here; see ref. 19) of the fly $G\alpha_q$, and PLCβ4 being the closest vertebrate homolog of the fly PLC (20, 21). The second mechanism has a ciliary motif (12), which we have first identified in M2- and M4-ipRGCs as follows: photoexcited melanopsin → $G\beta\gamma_q$ (i.e., the βγ partners of $G\alpha_q$, forming altogether the heterotrimeric G protein, G_q) → AC2* (potentially also AC4 and AC7, although still awaiting validation) → cAMP↑ → open HCN channels → membrane depolarization → action-potential firing (17, 18). This pathway is referred to here as the cAMP/HCN pathway. The exact subunit composition/stoichiometry of the native HCN channels in ipRGCs is still uncertain, but at least HCN4 appears to be a component (17, 18). One unusual feature of this second pathway is that, unlike cGMP being the predominant second messenger mediating ciliary phototransduction across the animal kingdom, cAMP is used in ipRGCs (17, 18) as in the jellyfish ciliary photoreceptor (22)—with a potentially important evolutionary

Author contributions: G.L. and K.-W.Y. designed research; G.L. performed research; G.L., L.C., and Z.J. analyzed data; L.C. and Z.J. offered some technical insights and experience; and G.L. and K.-W.Y. wrote the paper.

Reviewers: R.J.L., The University of Manchester; and A.T., Osaka Koritsu Daigaku.

The authors declare no competing interest.

[1]To whom correspondence may be addressed. Email: gli40@jhmi.edu or kwyau@jhmi.edu.

[2]Present address: Department of Neurobiology, Harvard Medical School, Boston, MA 02115.

[3]Present address: Department of Ophthalmology, Baylor College of Medicine, Houston, TX 77030.

This article contains supporting information online at https://www.pnas.org/lookup/suppl/doi:10.1073/pnas.2315282120/-/DCSupplemental.

Published December 18, 2023.

implication (17, 18). Another unusual feature is that it employs a cross-GPCR-motif signaling pathway by involving the direct activation of adenylyl cyclase (AC) by G_q's βγ-subunits instead of by $G\alpha_s$ and/or $G\alpha_{olf}$ (18). In ipRGCs, the PLCβ4/TRPC6,7 pathway has faster kinetics, whereas the cAMP/HCN pathway is slower so that, when operating together in the same cell upon light stimulation, the PLCβ4/TRPC6,7-mediated electrical response precedes the cAMP/HCN-mediated response albeit with substantial temporal overlap between the two (18). Every recorded M1-, M2-, and M4-cell appears to have both pathways, although with different percentage representations by each pathway across ipRGCs subtypes at response saturation so that not both responses are necessarily clearly visible (18). This co-existence of the two pathways in each cell breaks the general dogma about the segregation of the two signal-transduction motifs in separate cells among extant photoreceptors depending on whether the photosensitive compartment of a given photoreceptor type is microvilli- or cilium-derived (12, 17, 18).

In the current work, we examined the remaining subtypes of ipRGCs, namely, M3-, M5-, and M6-ipRGCs (4–11). These cells are present in far fewer numbers in the retina. Our question is whether they also use the same phototransduction mechanisms as we found in M1-, M2-, and M4-cells. Extrapolating from our findings on M1-, M2-, and M4-cells so far (17, 18), we speculated this to be the case, and indeed confirm it here. For proper comparison and characterization across all subtypes, we have also quantified the percentage representations by each pathway in saturated light responses (except for M6-cells, which are less photosensitive) from each ipRGC subtype.

Our overall phototransduction work on ipRGCs (16–18), including the current data, share only limited agreement with that from another group (23–25). This other group agreed on the existence of the PLCβ4/TRPC pathway, but has not clearly acknowledged the existence of a cyclic-nucleotide-mediated phototransduction pathway (23, 25).

Results

Similar Intrinsic Light Responses Broadly across M1- through M6-ipRGCs. We isolated the intrinsic light response of ipRGCs with synaptic blockers to eliminate all synaptic inputs from upstream rods and cones as well as their associated circuits (*SI Appendix, Materials and Methods*). Whole-cell, patch-clamp recordings were performed at 30 to 32 °C from individual ipRGCs, predominantly M3-, M5-, and M6-cells but also M1-, M2-, and M4-cells for the purpose of immediate comparison (with all recordings shown here being undertaken by one and the same person, GL). An *Opn4-tdTomato* mouse line (26) was used for all recordings from M1- through M5-cells, whereas a *Cdh3-GFP* line (11) was used largely for M6-cells (*SI Appendix, Materials and Methods*). Unless specified otherwise, 200-ms flashes (at 5-min intervals) of diffuse unattenuated white light (with infrared light removed by a water filter and the light spot spanning beyond the entire dendritic field of a recorded cell) were used to elicit bright responses from the cells. Based on the shape and kinetics of the responses, those from M3- and M5-cells should be at saturation, but the M6-response was probably not (Fig. 1, cf. dim-flash response in inset under M1-subtype). Given the presumably different densities of melanopsin on different ipRGC subtypes (based qualitatively on the immunolabeling intensity; see refs. 8 and 9), different numbers of photons are expected to be absorbed across subtypes even for the same incident light intensity. At the same time, the different ipRGC subtypes may also have different expression levels of the various transduction components downstream of melanopsin,

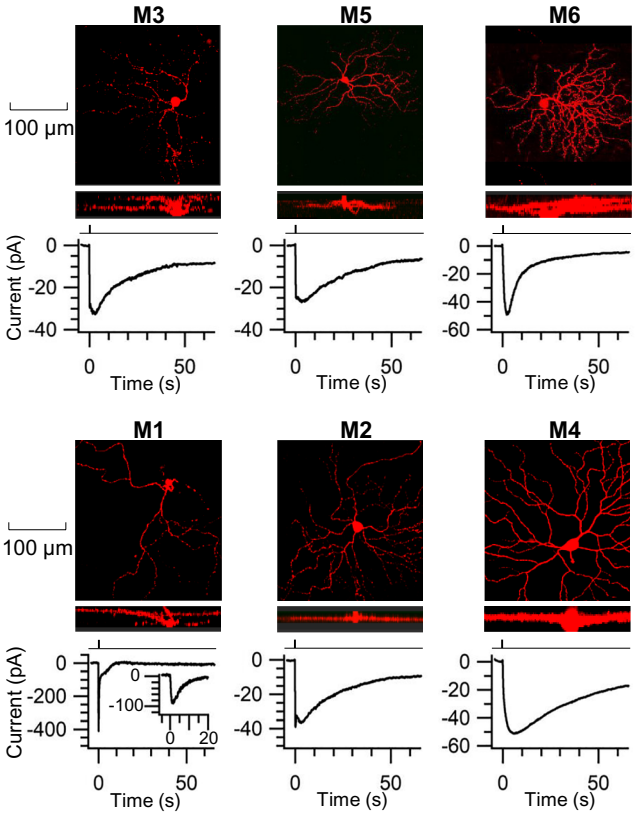

Fig. 1. Intrinsic saturated light responses (except for M6) across WT M1- through M6-ipRGCs. In each panel, top shows flat-mount view (stacked confocal image), middle shows the corresponding cross-sectional view of post-recording ipRGC filled with neurobiotin through recording pipette and visualized with cy3 streptavidin that binds to neurobiotin) in whole-mounted retina, and bottom shows cohort-averaged response (M3: n = 9, M5: n = 7, M6: n = 10, M1: n = 7, M2: n = 8, M4: n = 8). *Inset* in M1 panel shows a representative dim-flash response. Cells were targeted based on tdTomato or GFP signal in BAC transgenic *Opn4:tdTomato* or *Cdh3-GFP* strain, and identities were confirmed through post-hoc immunostaining of Alexa Fluor 568 Hydrazide routinely used in all experiments. Clamp voltage: −70 mV. Light stimulation: Full-field, 200-ms Xe white flash giving 2.1×10^{10} equivalent 480-nm photons μm^{-2} s^{-1}.

including the ion channel at the final step of phototransduction (i.e., TRPC6,7 channels or HCN channels), thus affecting the amplitude of the response (*Discussion*). In this work, we are concerned mostly with a qualitative characterization of the two phototransduction mechanisms in M3-, M5-, and M6-cells. A more detailed study of subtype sensitivity and response kinetics will be carried out separately down the road. After recording, the subtype identity of a recorded cell was verified by Alexa Fluor 568 hydrazide and often also by post hoc immunostaining of neurobiotin, both dialyzed into the cell from the whole-cell pipette. M3-cells were identified based on their bi-stratified dendrites in the ON- and OFF-sublaminar layers of the inner plexiform layer, together with a large dendritic field (Fig. 1, *Top Left*; for the exact quantification of the morphology, see ref. 8). M5-cells were identified based on their dendrites being stratified in the ON-sublaminar layer, together with a small somatic size and bushy dendritic field (Fig. 1, *Top Middle*; see ref. 10). M6-cells, like M3-cells, have bi-stratified dendrites in the ON- and OFF-sublaminar layers (Fig. 1, *Top Right*; see ref. 11), but have small somata and bushy dendritic fields. M1-, M2-, and M4-cells were identified as described previously (17).

The Fig. 1, *Bottom* in each ipRGC-subtype panel shows the ensemble-averaged intrinsic response (heretofore referred to simply as "response", understood to be intrinsic) to a bright flash (see

above paragraph regarding light intensity). The response of M3- and M5-cells, as that of M2-cells, exhibited two components: one with a fast rise that peaked early (fast component) followed by a second that peaked a little later and was accompanied by a slow decay (slow component). The fast peak was often not clearly visible, with the slow peak revealing itself merely as a transient, gradually rising "plateau" that decayed slowly afterward. The overall response thus resembled that of the M2-response. The M6-cell response was dominated by the fast-component, resembling to some degree the M1-cell's response to a relatively dim flash (see *Inset* in Fig. 1 underneath M1). WT M4-cells, as reported previously (17, 18), stood out by giving a light response composed predominantly of the slow component (Fig. 1).

Thus, overall, M3- and M5-cells responded largely like M2-cells, whereas M6-responses somewhat resembled poorly sensitive M1-responses. Next, we asked whether all subtypes have similar phototransduction mechanisms.

Involvement of G_q/PLCβ4/TRPC6,7 Pathway in Fast Component of M3-, M5-, and M6-Responses. We checked systematically the mechanism for the fast response component in M3-, M5-, and M6-ipRGCs. We started with the chemical YM-254890, which interfered with the activation of the $G\alpha_q$-subfamily (except for $G\alpha_{15}$, which reportedly is not affected by this chemical; see ref. 19) by inhibiting the GTP-for-GDP exchange in these proteins. Previously, it was shown that the entire response (i.e., both fast and slow components) of M2- and M4-cells essentially disappeared in the presence of 10-μM YM-254890 (18, 19; see Fig. 2*F* here). Here, we found the same for M1-, M3-, M5-, and M6-cells (Fig. 2 *B* and *F*, showing ensemble averages), indicating G_q-subfamily is required for both pathways. To remove G_q-subfamily signaling, we could also have used the $G\alpha_q^{fl/fl}$;$G\alpha_{11}^{-/-}$;$G\alpha_{14}^{-/-}$;*AAV2-CMV-Cre-GFP* genotype achieved by virally introduced Cre, as we did previously (17, 18). However, because M6-ipRGCs can only be identified within about 1 mo of the animal's birth (11) (*SI Appendix, Materials and Methods*), which may not be long enough for *AAV2-CMV-Cre-GFP* to take full effect unless the virus is injected soon after the animal's birth, we did not choose this option.

We next checked the requirement of PLCβ4 by using the PLCβ4-KO ($Plcb4^{-/-}$) mouse line. We found that the fast response component was selectively abolished in $Plcb4^{-/-}$ M3-, M5-, and M6-cells, leaving the slow component (Fig. 2*C*, showing ensemble-averages). Finally, we used the $Trpc6,7^{-/-}$ mouse line to check the involvement of the TRPC6 and TRPC7 channel isoforms. In this genotype, as in $Plcb4^{-/-}$, the fast response component of M3-, M5-, and M6-ipRGCs was specifically removed (Fig. 2*D*). This effect was not immediately obvious because the peak of the fast response component in WT M3- and M5-cells was mostly obscured by the temporally overlapping slow component (see earlier), and the low sensitivity of M6-cells (see earlier) rendered the fast component still far from saturation to show a fast peak (see also ref. 26). In principle, the genetic method of using the $Trpc6,7^{-/-}$ background for separating the fast and slow components would seem ideal. However, a more appropriate method will be described later. In short, only TRPC6 and TRPC7 from TRPC1-7 isoforms are specifically employed in the fast phototransduction pathway across all ipRGC subtypes.

Involvement of G_q/cAMP/HCN Pathway in Slow Component of M3-, M5-, and M6-Responses. The above effect of YM-254890 indicates that the G_q-subfamily also mediates the slow response component across all ipRGC subtypes. To check whether a cyclic nucleotide is involved in this pathway in M3-, M5-, and M6-cells, we dialyzed caged cAMP or cGMP (50-μM DEACM-cAMP or cGMP) from a whole-cell pipette into the soma of one of these recorded cells (with an $Opn4^{-/-}$ background to avoid the confounding effect of melanopsin activation) and did photo-uncaging over the soma with a 1-s white flash (40-μm spot) from a mercury arc lamp (17, 18) (*SI Appendix, Materials and Methods*). M3-, M5-, and M6-cells all gave a response to uncaged cAMP but not to uncaged cGMP (for M6, the downward trend of the recording actually started before the uncaging flash for cGMP; see *Insets*) (Fig. 3). The same uncaging experiment on M1-, M2-, and M4-cells are also shown for comparison (Fig. 3). M1-cells gave essentially no response, while M2-cells gave a response to uncaged cAMP but not cGMP. M4-cells, on the other hand, responded to both uncaged cAMP and cGMP (especially cAMP). The M1-, M2-, and M4-cells behaved as what we have found previously (17). In short, M3- and M5-cells broadly resembled M2-cells, whereas M6-cells resembled weakly sensitive M1-cells. Recently, we have studied M4-cells quite extensively and demonstrated that cAMP is indeed the second messenger mediating the slow response, via direct activation of AC by $G\beta\gamma_q$ (18). We did not repeat these earlier experiments on other ipRGCs here because their procedures and reasoning are fairly elaborate, but instead jumped to the step of checking AC as the effector enzyme in the slow response pathway.

From our previous experiments on M4-cells, we showed by using the AC2-KO genotype ($Adcy2^{-/-}$) that AC2 (a member of Group II ACs, which include AC2, AC4, and AC7; see refs. 27 and 28) participates in phototransduction underlying the slow response of M4-cells (18). We checked here the other ipRGC subtypes with the same $Adcy2^{-/-}$ genotype in the presence of the TRPC channel inhibitor, 20-μM Ruthenium Red (RR), to remove the confounding intrinsic fast-response component (17, 29). We found that the slow response of $Adcy2^{-/-}$ M3-cells was ~1/3 smaller than control (ensemble average; Fig. 4*B* and statistics in Fig. 4*E*). A very similar reduction was found for M5-cells (Fig. 4*B* and statistics in Fig. 4*E*), and a slightly larger reduction for M6-cells (Fig. 4*B* and statistics in Fig. 4*E*). For M1-cells, no obvious effect of $Adcy2^{-/-}$ was observed (Fig. 4 *G* and *J*), while $Adcy2^{-/-}$ M2-cells lost about 1/3 of the control response (Fig. 4 *G* and *J*). For M4-cells, the effect of $Adcy2^{-/-}$ was milder than previously observed (probably due to variations across light sources in different set-ups), being reduced by at most 1/4 (Fig. 4 *G* and *J*).

We also successfully revived the $Adcy4^{-/-}$ and $Adcy7^{fl/fl}$ (30) mouse lines originally generated by others (*Acknowledgments* and *SI Appendix, Materials and Methods*), and virally introduced Cre-GFP into the $Adcy7^{fl/fl}$ mouse eye to get the AC7-KO mice ($Adcy7^{fl/fl}$;*AAV-CMV-Cre-GFP*) (*SI Appendix, Materials and Methods*). Overall, the effect of $Adcy4^{-/-}$ on the various subtypes was broadly similar to the effect of $Adcy2^{-/-}$ (Fig. 4 *C* and *H* and statistics in Fig. 4 *E* and *J*; see legend). The same was true for $Adcy7^{fl/fl}$;*AAV-CMV-Cre-GFP* (Fig. 4 *D* and *I* and Fig. 4 *E* and *J*). For this last genotype, we were unable to examine M6-cells with the same strategy, due to the issue mentioned earlier that the viral transfection has to be carried out very early after animal birth. However, by using virus on the *OPN4-tdTomato* mouse line, we did manage in rare cases to encounter occasional $Adcy7^{fl/fl}$;*AAV-CMV-Cre-GFP* M6-cells (9, 31).

We also examined the $Adcy2^{-/-}$;$Adcy4^{-/-}$ and $Adcy2^{-/-}$ $Adcy7^{fl/fl}$;*AAV-CMV-Cre-GFP* double-KO genotypes (*SI Appendix*, Fig. S1). Overall, the double-KO data showed no clear additive effect between AC2 and AC4, or between AC2 and AC7. We have not yet examined $Adcy4^{-/-}$;$Adcy7^{fl/fl}$;*AAV-CMV-Cre-GFP* double-KOs. Most importantly, the $Adcy2^{-/-}$;$Adcy4^{-/-}$; $Adcy7^{fl/fl}$; *AAV-CMV-Cre-GFP* triple-KO line will be informative when ready, indicating whether the slow light-response indeed completely disappears or not.

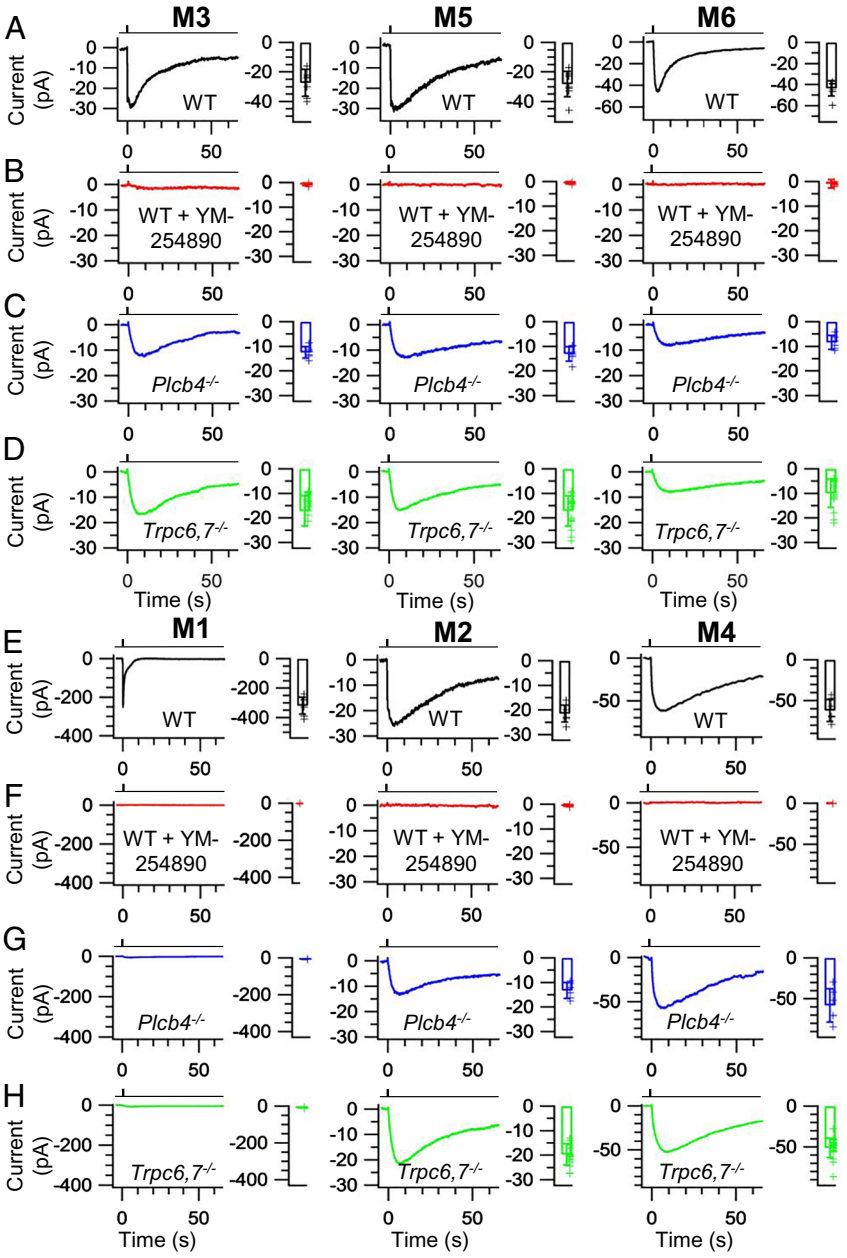

Fig. 2. G_q/PLCB4/TRPC6.7 signaling underlying fast light-response component. (*A–D*) Cohort-averaged intrinsic light responses and their associated collective data (transient-peak amplitude ± SD) of M3-, M5-, and M6-ipRGCs in WT (*A*), WT with 10-μM YM-254890 (*B*), *Plcb4*$^{-/-}$ (*C*), and *Trpc6,7*$^{-/-}$ (*D*). M3: WT: 29.30 ± 8.25 pA, n = 10; WT+YM drug: 0.68 ± 0.55 pA, n = 9; *Plcb4*$^{-/-}$: 12.49 ± 2.29 pA, n = 7; *Trpc6,7*$^{-/-}$: 17.10 ± 8.10 pA, n = 20. M5: WT: 30.33 ± 8.23 pA, n = 9; WT+YM drug: 0.51 ± 0.54 pA, n = 8; *Plcb4*$^{-/-}$: 13.10 ± 2.92 pA, n = 7; *Trpc6,7*$^{-/-}$: 17.09 ± 6.22 pA, n = 20. M6: WT: 43.60 ± 7.29 pA, n = 8; WT+YM drug: 0.86 ± 0.75 pA, n = 8; *Plcb4*$^{-/-}$: 8.40 ± 2.85 pA, n = 6; *Trpc6,7*$^{-/-}$: 9.97 ± 5.78 pA, n = 17. (*E–H*) Cohort-averaged intrinsic light responses and associated collective data (transient-peak amplitude ± SD) of M1-, M2-, and M4-ipRGCs in WT (*E*), WT with 10-μM YM-254890 (*F*), *Plcb4*$^{-/-}$(*G*) and *Trpc6,7*$^{-/-}$ (*H*). M1: WT: 319.38 ± 57.26 pA, n = 10. WT+YM drug: 0.74 ± 0.51 pA, n = 8; *Plcb4*$^{-/-}$: 6.29 ± 1.94 pA, n = 7; *Trpc6,7*$^{-/-}$: 7.53 ± 2.91 pA, n = 14. M2: WT: 25.31 ± 3.39, n = 8; WT+YM drug: 0.39 ± 0.44 pA, n = 8; *Plcb4*$^{-/-}$: 13.28 ± 3.28 pA, n = 6; *Trpc6,7*$^{-/-}$: 19.63 ± 4.40 pA, n = 19. M4: WT: 62.14 ± 5.52 pA, n = 7; WT+YM drug: 0.14 ± 0.20 pA, n = 7; *Plcb4*$^{-/-}$: 58.00 ± 20.42 pA, n = 6; *Trpc6,7*$^{-/-}$: 50.99 ± 11.81 pA, n = 21.Clamp voltage: −70 mV. Light stimulation: Full-field, 200-ms Xe white flash giving 2.1 × 10^{10} equivalent 480-nm photons μm^{-2} s^{-1}.

Finally, we asked whether HCN channels constitute the final stage of phototransduction underlying the slow-response component. Previously, in M1-, M2-, and M4-cells, we found that the specific HCN channel inhibitor, ZD7288 (50 μM), in the bath solution blocked the HCN current in the *Trpc6,7*$^{-/-}$ retina (17; see also refs. 32 and 33). We found the same here for M3-, M5-, and M6-cells (n = 14, 14, and 7, respectively, albeit incompletely for M3- and M5-cells; Fig. 5*A*). Second, HCN channels are known to be opened by both cyclic nucleotides and hyperpolarization (34, 35). As we previously reported, membrane hyperpolarization reduced the light response of *Trpc6,7*$^{-/-}$M2-cells by half (17), consistent with the expected reduction in cAMP modulation of HCN channel at different clamp voltages (35). We examined this property of the light response from *Trpc6,7*$^{-/-}$M3-, M5-, and M6-cells, and found the response at -100 mV to decrease to approximately 1/3 in M3- (n = 13), to nearly half in M5- (n = 12) and to under 1/3 in M6-cells (n = 8) from that at −70 mV (Fig. 5*B*), broadly similar to that found in M2-cells (17).

Separation of Fast and Slow Response Components in Different ipRGC Subtypes. To quantify the percentage representation by each phototransduction pathway in a given ipRGC subtype, a simple approach might have been to record from ipRGCs of the TRPC6- and TRPC7- double KO (*Trpc6,7*$^{-/-}$) mouse line,

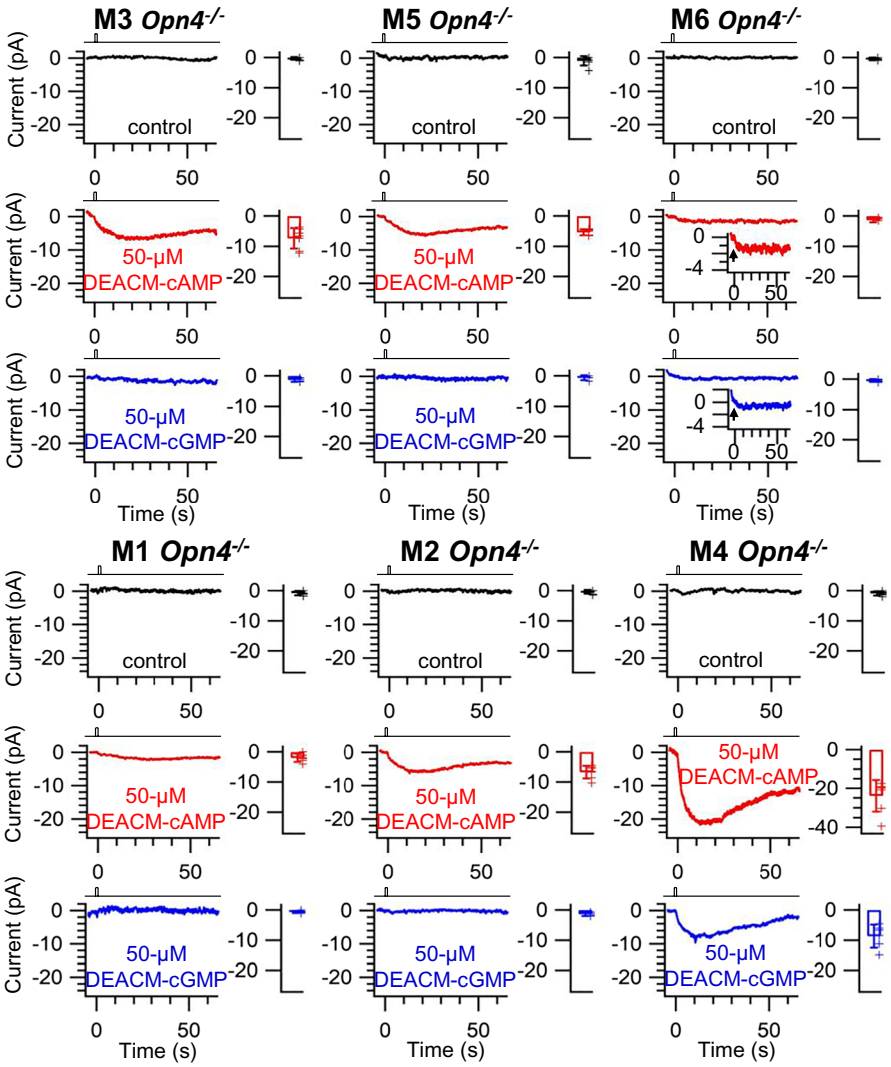

Fig. 3. cAMP/HCN signaling underlying slow light-response component. Cohort-averaged responses to intracellular photo-uncaged cAMP or cGMP and their associated collective data (transient-peak amplitude ± SD). All experiments in *Opn4*$^{-/-}$ genetic background to remove endogenous light response. For each ipRGC subtype, *Top* shows absence of caged cyclic nucleotide (control), *Middle* shows presence of 50-μM DEACM-cAMP, and *Bottom* shows presence of 50-μM DEACM-cGMP.M3: control: 0.32 ± 0.50 pA, n = 6; DEACM-cAMP: 7.39 ± 3.37 pA, n = 7; DEACM-cGMP: 1.38 ± 0.61 pA, n = 4. M5: control: 1.09 ± 1.57 pA, n = 7; DEACM-cAMP: 5.40 ± 1.03 pA, n = 7; DEACM-cGMP: 0.60 ± 0.85 pA, n = 4. M6: control: 0.42 ± 0.43 pA, n = 5; DEACM-cAMP: 1.08 ± 0.61 pA, n = 5, shown amplified in *Inset*; DEACM-cGMP: 0.47 ± 0.45 pA, n = 6, shown amplified in *Inset*. M1: control: 0.80 ± 0.70 pA, n = 6; DEACM-cAMP: 2.05 ± 1.40 pA, n = 6; DEACM-cGMP: 0.62 ± 0.41 pA, n = 6. M2: control: 0.39 ± 0.66 pA, n = 7; DEACM-cAMP: 6.77 ± 2.12 pA, n = 7; DEACM-cGMP: 1.38 ± 0.61 pA, n = 4. M4: control: 0.95 ± 0.71 pA, n = 6; DEACM-cAMP: 23.78 ± 8.08 pA, n = 7; DEACM-cGMP: 8.65 ± 3.82 pA, n = 6. Clamp voltage: −70 mV. Photo-uncaging light: 40-μm diameter, 1-s white light spot at 0.12-μW μm^{-2} from a mercury arc lamp centered at the soma.

thereby eliminating the fast PLCβ4/TRPC6,7 phototransduction pathway in order to isolate the slow cAMP/HCN pathway. By subtracting the ensemble average response associated with the isolated cAMP/HCN pathway from that associated with the WT composite response, one could obtain the PLCβ4/TRPC6,7 response. However, the disadvantage of this approach is that it involves the subtractive difference between the averaged responses from two cohorts of cells with different genotypes. Thus, any cell-to-cell variation in response amplitude within each genotype, which indeed exists, would affect the calculations.

One way that avoids the confounding effect of subtraction across genotypes is to study WT ipRGCs and utilize RR, an inhibitor of TRPC channels (17), in the bath solution to remove the fast component within a given genotype. To check whether RR also affects the HCN current, we isolated the slow response component with the *Trpc6,7*$^{-/-}$ genotype and applied 20-μM bath RR to each ipRGC subtype. Its effect was quite uniform across subtypes (Fig. 6), leading to a slightly smaller slow response that varied between 0.84 and 0.92 of control (at peak). We used its mean of 0.89 (± 0.04, SD) as a correction below.

Given the above, we separated the fast and slow response components in each ipRGC subtype as follows. Starting with a WT ipRGC subtype (Fig. 7, *Top* panel under each ipRGC subtype), we used 20-μM bath RR to remove the PLCβ4/TRPC6,7-mediated fast response component (Fig. 7, *Middle* panel under each ipRGC subtype: red trace labeled "RR"). After correcting for the small effect of 20-μM RR on the HCN channel described above (i.e., dividing by 0.89), we obtained the true slow response component mediated by the cAMP/HCN pathway (Fig. 7, *Middle* panel under each ipRGC subtype: blue trace labeled "RR corrected"). Subtracting this component from the control composite response (Fig. 7, *Top* panel under each ipRGC subtype), we obtained the PLCβ4/TRPC6,7-mediated fast response component (Fig. 7, *Bottom* panel under each ipRGC subtype: green trace). The transient-peak amplitude of the extracted slow component divided by that of the overall composite response gives the percentage of

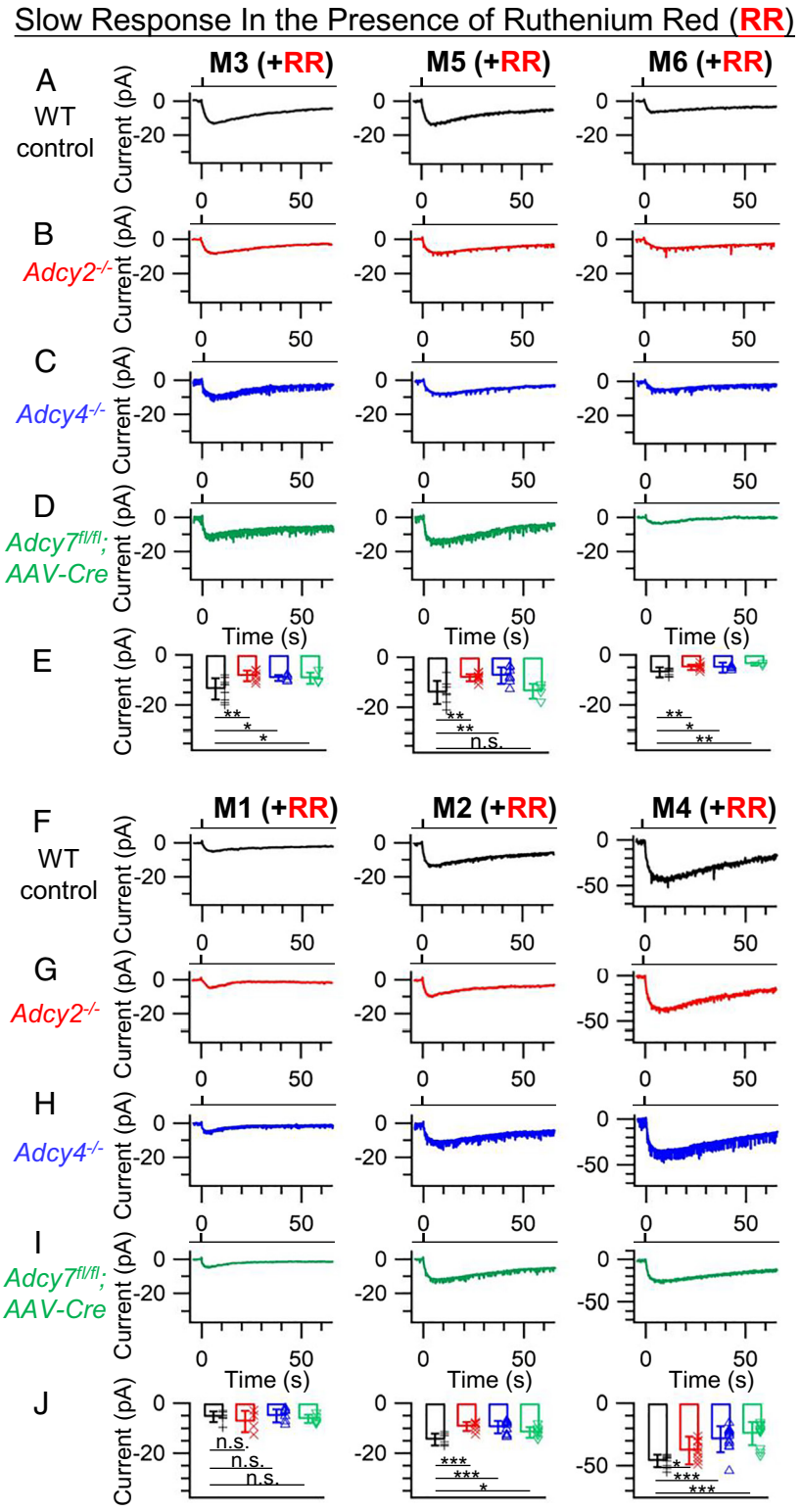

Fig. 4. AC2, AC4, and AC7 all involved in slow light-response component. All experiments in the presence of 20-μM RR to remove fast-response component. During RR perfusion, the presence of action potentials was commonly observed. (*A–E*) Cohort-averaged intrinsic light responses of M3-, M5-, and M6-ipRGCs and their associated collective data (transient-peak amplitude ± SD), in WT control (black), *Adcy2*$^{-/-}$(red), *Adcy4*$^{-/-}$(short for *Adcy4*^{tm1Dgen}, blue), and *Adcy7*$^{fl/fl}$; *AAV-Cre* (short for *AAV2-CMV-Cre-GFP*, green) mice. M3: WT control: 13.58 ± 4.20 pA, n = 10; *Adcy2*$^{-/-}$: 8.41 ± 2.13 pA, n = 6; *Adcy4*$^{-/-}$: 9.24 ± 1.22 pA, n = 4. *Adcy7*$^{fl/fl}$; *AAV-Cre*: 9.40 ± 2.28 pA, n = 5. M5: WT control: 14.26 ± 5.77 pA, n = 9; *Adcy2*$^{-/-}$: 8.10 ± 1.43 pA, n = 10; *Adcy4*$^{-/-}$: 7.33 ± 3.31 pA, n = 8; *Adcy7*$^{fl/fl}$; *AAV-Cre*: 13.65 ± 3.01 pA, n = 4. M6: WT control: 6.93 ± 1.95 pA, n = 8; *Adcy2*$^{-/-}$: 4.94 ± 1.06 pA, n = 8; *Adcy4*$^{-/-}$: 5.14 ± 2.01 pA, n = 4; *Adcy7*$^{fl/fl}$; *AAV-Cre*: 3.20 ± 0.68 pA, n = 2. (*F–J*) Same format as in *A–E*, except for M1-, M2-, and M4-cells. M1: WT control: 5.04 ± 1.18, n = 5; *Adcy2*$^{-/-}$: 7.38 ± 4.31, n = 6; *Adcy4*$^{-/-}$: 5.07 ± 2.61, n = 7; *Adcy7*$^{fl/fl}$; *AAV-Cre*: 6.28 ± 1.69, n = 7. M2: WT control: 14.59 ± 3.22, n = 7; *Adcy2*$^{-/-}$: 9.31 ± 1.71, n = 7; *Adcy4*$^{-/-}$: 9.59 ± 2.45, n = 11; *Adcy7*$^{fl/fl}$; *AAV-Cre*: 11.75 ± 4.24, n = 8. M4: WT control: 46.11 ± 7.03, n = 9; *Adcy2*$^{-/-}$: 37.74 ± 11.06, n = 9; *Adcy4*$^{-/-}$: 29.84 ± 10.30, n = 11; *Adcy7*$^{fl/fl}$; *AAV-Cre*: 24.37 ± 9.23, n = 12. $P < 0.005$. *$P < 0.05$, **$P < 0.01$, ***$P < 0.005$, n.s., not statistically different. *P*-values are from the *t* test with comparison to control. Clamp voltage: −70 mV. Light stimulation: A full field of 200-ms Xe white light flash (equivalent to 2.1×10^{10} photons μm^{-2} s^{-1} of 480-nm light).

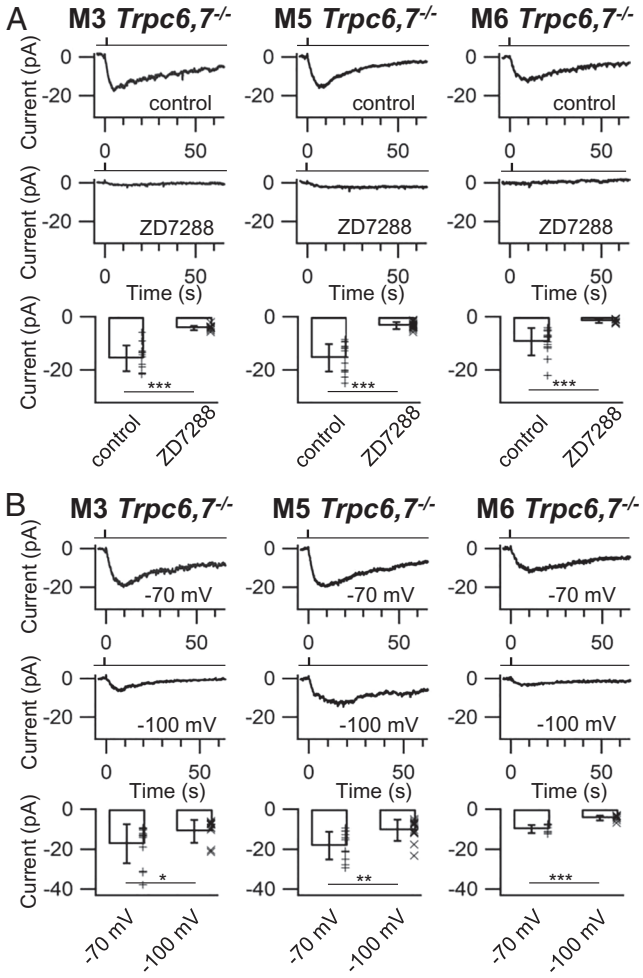

Fig. 5. Pharmacological evidence that HCN channel is involved in slow light-response component of M3-, M5-, and M6-ipRGCs. All experiments in *Trpc6,7*$^{-/-}$ genetic background to eliminate fast light-response component. (*A*, *Top* and *Middle*) Intrinsic light responses from the same cell in the absence (control) and presence of ZD7288, together with collective data (*Bottom*, transient-peak amplitude ± SD). M3: control: 15.63 ± 3.55 pA, n = 14; ZD7288: 4.14 ± 0.84 pA, n = 14. M5: control: 15.38 ± 1.65 pA, n = 16; ZD7288: 3.25 ± 1.28 pA, n = 14. M6: control: 9.35 ± 5.13 pA, n = 13; ZD7288: 1.56 ± 0.69 pA, n = 7. Clamp voltage: −70 mV. (*B*) Effect of membrane voltage. Same as in *A* but no 50-μM ZD7288. (*Top* and *Middle*) −70 mV vs. −100 mV. Sample recordings from single cells together with collective data (*Bottom*, transient-peak amplitude ± SD). M3: −70 mV, 17.29 ± 10.44 pA; −100mV, 11.09 ± 7.54 pA, n = 13. M5: −70 mV, 18.31 ± 6.88 pA; −100mV, 10.50 ± 5.33 pA, n = 12. M6: −70 mV, 9.94 ± 2.07 pA; −100mV, 4.53 ± 1.25 pA, n = 8. $P < 0.005$. *$P < 0.05$, ***$P < 0.005$, n.s., not statistically different. *P*-values are from the *t* test with comparison to control. Light stimulation: A full field of 200-ms Xe white light flash (equivalent to 2.1×10^{10} photons μm^{-2} s^{-1} of 480-nm light).

response attributed to the slow component (bottom panel under each subtype, indicated in blue color). How each response component results in signaling to the brain will depend on the action-potential firing triggered by the receptor current in each ipRGC subtype in native conditions.

The overall amplitude of the composite response at transient peak varied across ipRGC subtypes, being 319.38 ± 57.26 pA, n = 8 (mean ± SD) for M1-cells, 25.34 ± 4.33 pA, n = 8 for M2-cells, 29.3 ± 9.09 pA, n = 10 for M3-cells, 62.14 ± 13.40 pA, n = 7 for M4-cells, 30.26 ± 9.28 pA, n = 8 for M5-cells, and 43.60 ± 7.29 pA, n = 8 for M6-cells. The corresponding percentage representations of the slow component were: 2 % (M1), 63 % (M2), 51 % (M3), 81 % (M4), 52 % (M5), and 15 % (M6) of the total (i.e., composite) response. Because the fast and slow components had different transient-peak times, it may be more useful to compare them in terms of total charge transfer (i.e., membrane current integrated over time, up to the end of each digitized trace in Fig. 7 (~66 s after light stimulus). As such, the corresponding percentage representations of the slow component were: 30 % (M1), 72 % (M2), 82 % (M3), 76 % (M4), 59 % (M5), and 29 % (M6) of the total (see pie chart in *SI Appendix*, Fig. S2). The rather significant percentage differences in transient-peak response amplitude vs. total charge transfer have to do with the fact that the slow-response component lasts much longer. This may also be relevant when considering action-potential firing resulting from the photoresponses.

Reversal Potential of the Slow Response Component. In contrast to our previous (17, 18) and present findings, Sonoda et al. and Contreras et al. (23–25) suggested that the M4-cell's slow response component came instead from a light-suppressed dark K^+ leak through K2P TASK channels, with a reversal potential for the response being -90 mV. Accordingly, we checked the reversal potential of the slow response component in different ipRGC subtypes after isolating it with the *Trpc6,7*$^{-/-}$ background. In all subtypes (except for M1-cells, which were not studied because of their very small slow response component), the reversal potential was around 0 mV (Fig. 8*A*), as expected from HCN channels being permeable to both Na^+ and K^+. These data ruled out the involvement of K channels. At the same time, whether inward or outward depending on membrane voltage, the current response was largely eliminated by ZD7288 (Fig. 8*B*; control shown in red and ZD7288 action shown in blue), consistent with HCN channels' pharmacology. For M4-cells, we were able to reverse the response only in 9 out of 75 cells, possibly because of their large dendritic-field sizes and therefore space-clamp problems. For M5-cells, the light response could be reversed in ~50 % of the cells. For the remaining subtypes, the response could be reversed in all cells.

We have done the same experiments on *Opn4*$^{-/-}$ M3-, M4-, and M5-ipRGCs with photo-uncaging of cAMP in these cells and obtained similar results, namely, a reversal potential near 0 mV and an outward current at a positive voltage (*SI Appendix*, Fig. S3). In this case, the percentage of response reversal for M4-cells was ~60 % (8 out of 14 cells), and almost 100% for M3- and M5-cells.

Incidentally, Sonoda et al. and Contreras et al. (23–25) have not provided a mechanism by which light suppresses the K2P TASK channels or demonstrated the physical presence of these channels in M4-cells by other means such as observing a null phenotype in a gene-knockout mouse line. In contrast, the presence of HCN channels in RGCs is well known (17, 32, 33), as is their modulation by cAMP (32, 33).

Time Discrepancy in ZD7288 Blockage of I_h and of Its cAMP-Induced Current. A separate observation by the same group above (25) was that ZD7288 blockage of the hyperpolarization-activated I_h current in M4-ipRGCs occurred earlier than its blockage of the light response, which these authors took as evidence against HCN channels underlying the slow light-response component.

We confirmed this time discrepancy in an *Opn4*$^{-/-}$ M4-ipRGC, using photo-uncaged cAMP as a substitute for light in native phototransduction. In Fig. 9 *A*, *Top Left*, a step membrane hyperpolarization from −70 mV to −120 mV activated an inward I_h current (red arrowhead). Upon returning to −70 mV, a transient tail current was observed (blue arrowhead). At ~7 min after the addition of 50-μM bath ZD7288, both the inward current during hyperpolarization and the tail current upon repolarization disappeared, indicating the blockage of the I_h current (Fig. 9 *A*, *Top Middle*). In Fig. 9 *A*, *Bottom Left*, a photo-uncaged pulse of cAMP inside the cell at −70 mV activated a transient inward current. However, this inward current was only moderately reduced at ~7 min after the presence of ZD7288 (Fig. 9 *A*, *Bottom Middle*). At ~20 min after the presence

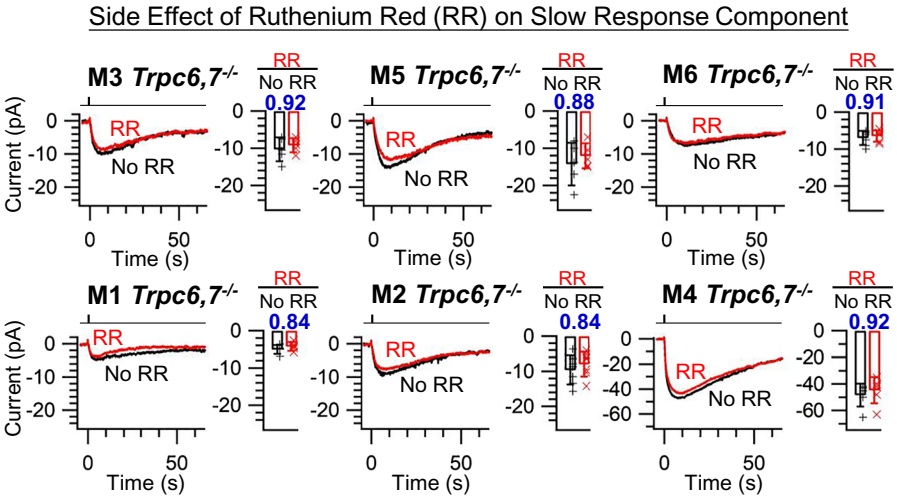

Fig. 6. Checking side-effect of RR on slow light-response component. Cohort-averaged intrinsic light responses of M1- through M6-ipRGCs in *Trpc6,7*$^{-/-}$ background and collective data (transient-peak amplitude ± SD). No RR (black) or 20-μM RR for 20 min (red). M3: no RR: 10.32 ± 3.26 pA, n = 5; RR: 9.20 ± 1.90 pA, n = 5. M5: no RR: 14.26 ± 5.77 pA, n = 5; RR: 12.06 ± 3.35 pA, n = 5. M6: no RR: 6.93 ± 1.95 pA, n = 7; RR: 6.42 ± 1.53 pA, n = 6. M1: no RR: 5.04 ± 1.18 pA, n = 5; RR: 4.26 ± 1.16 pA, n = 5. M2: no RR: 9.61 ± 4.16 pA, n = 7; RR: 8.00 ± 3.52 pA, n = 7. M4: no RR: 48.33 ± 8.62 pA, n = 6; RR: 44.67 ± 9.91 pA, n = 6. Clamp voltage: −70 mV. Light stimulation: Full-field, 200-ms Xe white light flash equivalent to 2.1 × 10^{10} photons μm^{-2} s^{-1} of 480-nm light.

of ZD7288, the photouncaged-cAMP-induced inward current finally completely disappeared (Fig. 9 *A*, *Bottom Right*). Thus, it required roughly twice as much time to inhibit the cAMP-induced current as to inhibit the I_h current.

Nonetheless, rather than taking the above observation as evidence that the cAMP-triggered current (equivalent to the slow intrinsic light-response component) was distinct from the I_h (HCN) current, our thinking is that the ZD7288 happened to

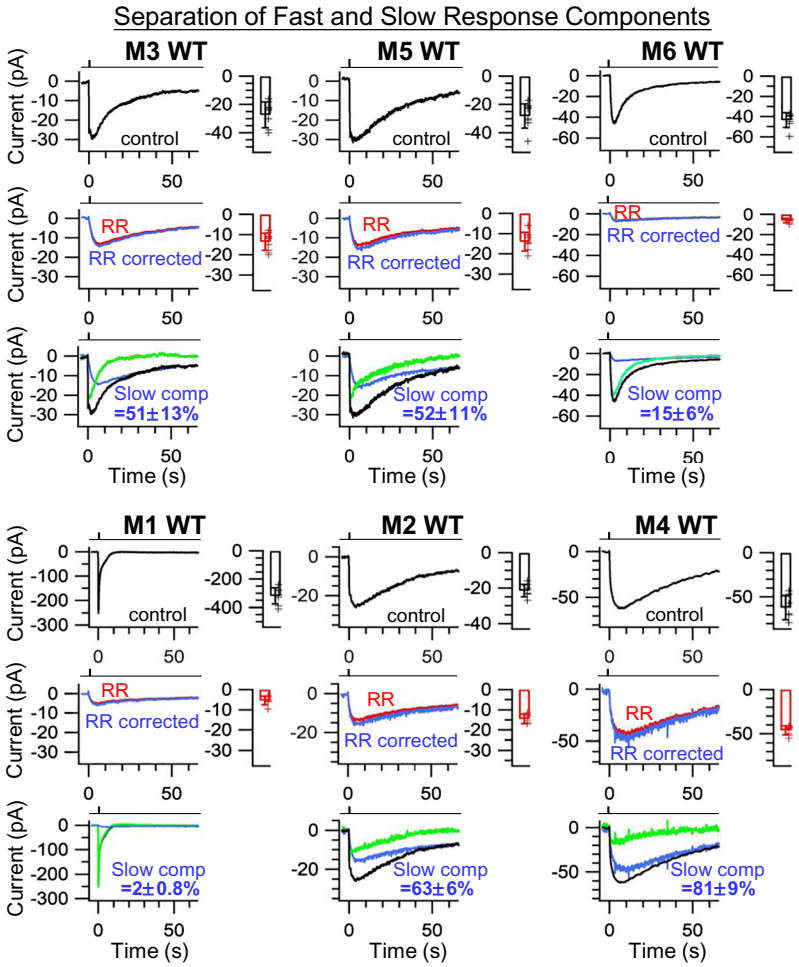

Fig. 7. Fast and slow light-response components separated by RR. Cohort-averaged intrinsic light responses and collective data (transient-peak amplitude ± SD) of M1- through M6-ipRGCs. WT genetic background. Responses in top row here are identical to those in Fig. 2 *A* and *E*. See text for details. Clamp voltage: −70 mV. Light stimulation: Full-field, 200-ms Xe white light flash, equivalent to 2.1 × 10^{10} photons μm^{-2} s^{-1} of 480-nm light.

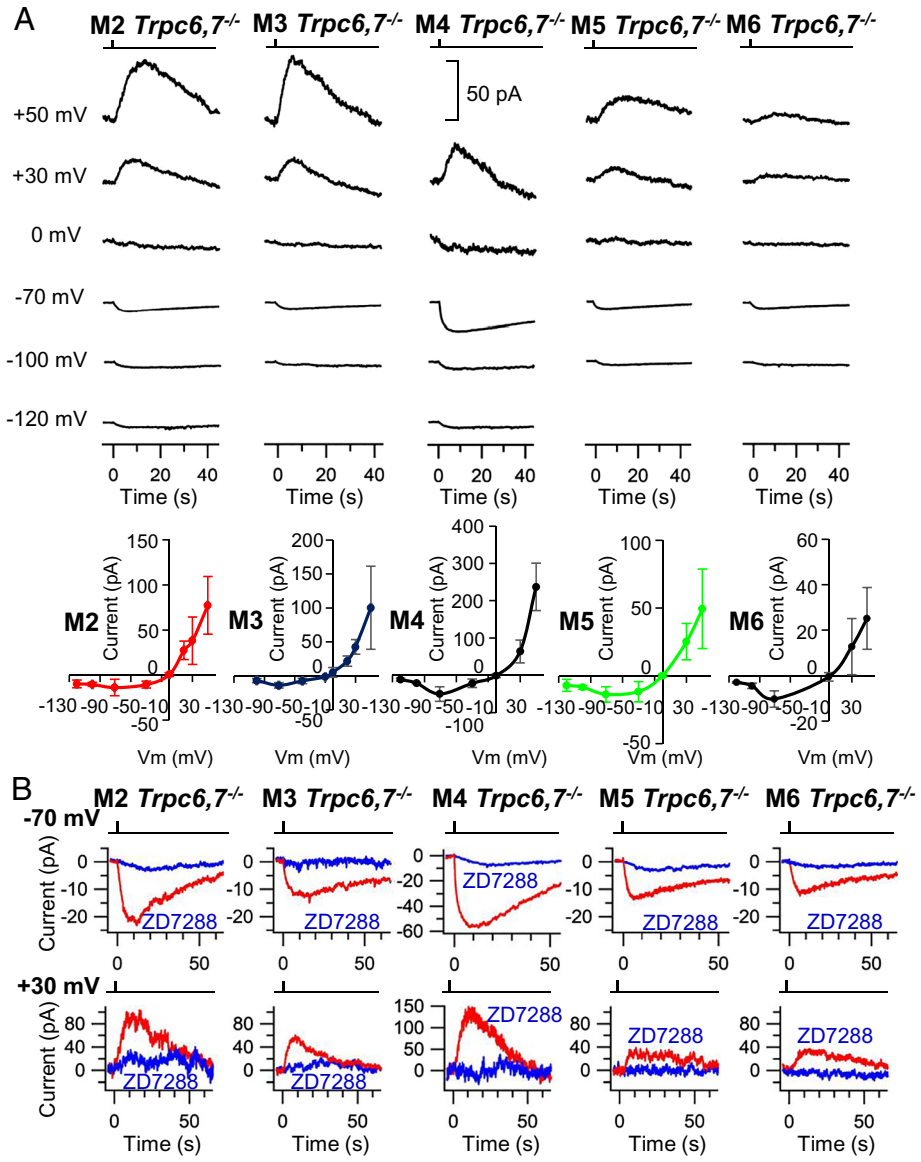

Fig. 8. Reversal potential of slow light-response component close to 0 mV. *Trpc6,7*$^{-/-}$ genetic background throughout. (*A*) Cohort-averaged responses at different holding voltage (*Top*) and the corresponding I-V relation (*Bottom*) of M2-, through M6-ipRGCs. M1-response, with a very small outward currents, is not included. (*B*) Response is sensitive to ZD7288 (red: control; blue: 50-μM ZD7288) whether inward (−70 mV) or outward (+30 mV). Light stimulation: Full-field, 200-ms Xe white light flash (equivalent to 2.1 × 10^{10} photons μm^{-2} s^{-1} of 480-nm light).

require different times to produce one effect or another. After all, the gating of the HCN channel by membrane hyperpolarization may not be the same as its modulation by cAMP. To confirm this idea in a simpler system, we expressed HCN channels in HEK293 cells. We used the (human) hHCN4 isoform because our previous work (17) indicated that mouse ipRGCs have at least HCN4; thus, the behavior of HCN4 is probably more akin to our experiments here than other HCN isoforms. When expressed, the open probability of hHCN4 channels increases progressively from −40 mV to −120 mV (35).

In Fig. 9*B*, we carried out the same experiment as in Fig. 9*A*, except that the recording was made from HEK293 cells transfected with hHCN4. We basically found the same result as in Fig. 9*A*, i.e., a time delay in the ZD7288-blockage of the cAMP-induced inward current compared to the ZD7288-blockage of the I_h current. However, one important difference between Fig. 9 *A* and *B* is that, whereas the intrinsic phototransduction channels in ipRGCs may not be construed to be identical to hHCN4, in the case of HEK293 cells we have transfected only with hHCN4. In other words, the time discrepancy in the ZD7288-blockage of the cAMP-induced inward current compared to the ZD7288-blockage of the I_h current had to reside in the same channel molecules. At this point, the exact mechanism underlying the time discrepancy is unknown.

Discussion

Fig. 10 shows a summary diagram of phototransduction in ipRGCs, depicting the rhabdomeric and the ciliary signaling pathways operating in parallel and their relative contributions (in terms of integrated charge transfer) to the saturated (except for M6-cells) light response in each subtype.

The overall conclusion from this and the preceding (18) work is simple; namely, all ipRGC subtypes (M1 through M6) identified so far make use of the same phototransduction mechanisms for signaling light. As such, this situation is similar to that for rods and cones. In Results, we have addressed a couple of key points made by Contreras et al. 2022 (25) against HCN channels mediating the slow response

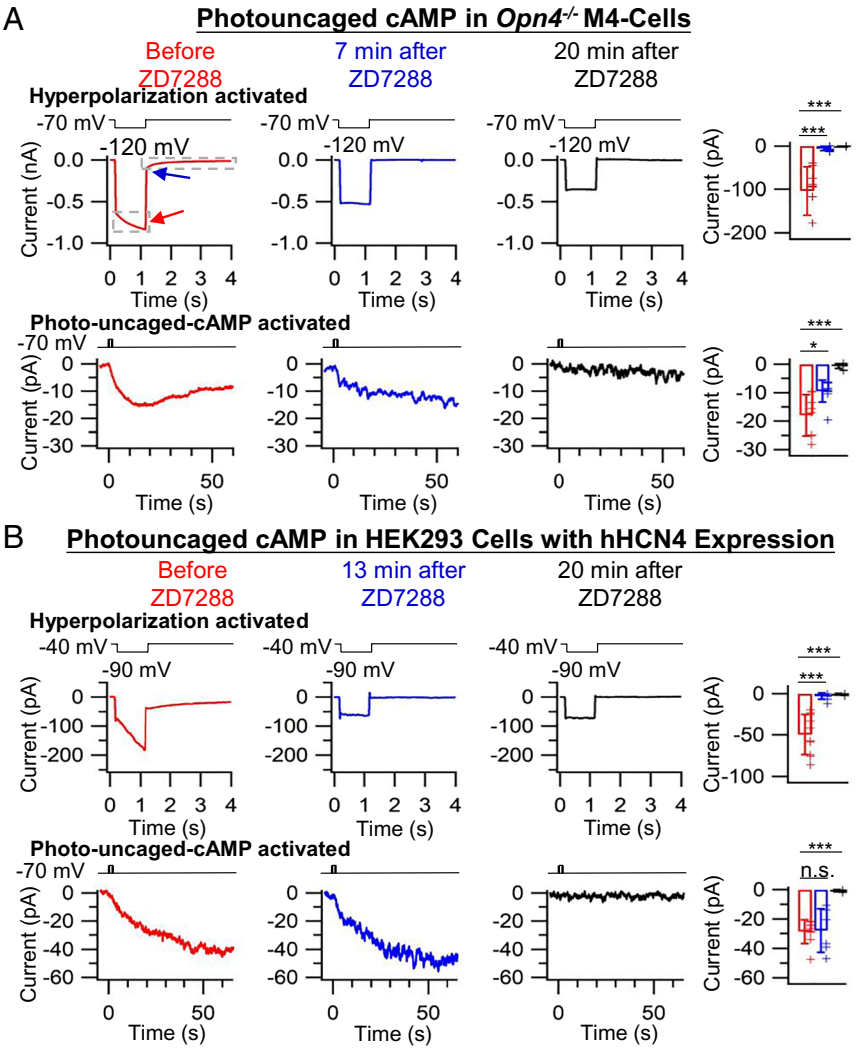

Fig. 9. Temporal difference in ZD7288 effect on I_h current and photouncaged-cAMP-induced current. (*A*, *Top*) Cohort-averaged I_h current evoked after a 1-s pulse to −120 mV in *Opn4*$^{-/-}$M4-cells before ZD7288 (*Left*), 7 min after 50-μM ZD7288 (*Middle*), and 20 min after 50-μM ZD7288 (*Right*). Collective data, ± SD (far right). (*Bottom*) Cohort-averaged response to photouncaged cAMP before ZD7288 (*Left*), 7 min after ZD7288 (*Middle*), and 20 min after ZD7288 (*Right*). Collective data (transient peak ± SD) (far right). (*B*) Same experiment but on a HEK293 cell transfected with hHCN4. (*Top*) Cohort-averaged I_h current evoked after a 1-s pulse to −90 mV before ZD7288 (*Left*), 13 min after 50-μM ZD7288 (*Middle*) and 20 min after 50-μM ZD7288 (*Right*). Collective data, ± SD (far right). (*Bottom*) Cohort-averaged response to photouncaged cAMP before ZD7288 (*Left*), 13 min after ZD7288 (*Middle*) and 20 min after ZD7288 (*Right*). Collective data (transient peak ± SD) (far right). Photouncaging light: 40-μm, 1-s white light spot (0.12-μW μm^{-2}) centered at the soma from a mercury arc lamp.

component. They further presented as supporting evidence their observation that the amplitude of the tail current upon stepping back from −120 mV to −70 mV in M2- and M4-ipRGCs did not differ in the presence or absence of light (see their Figs. 4 and 2). However, it needs to be noted that, at least for HCN4, the I_h current appears to already reach near maximum at −120 mV (see ref. 35), thus the positive modulation by cAMP may not increase the current further.

A contrast between ipRGC subtypes and rods/cones should be pointed out nonetheless. Despite rods and cones share the same phototransduction mechanism—a ciliary pathway involving a cGMP-phosphodiesterase as the effector enzyme that hydrolyzes cGMP to close CNG channels—the underlying transduction components do show their distinct rod- vs. cone-molecular isoforms. Besides their distinct pigments for the obvious purpose of differential spectral detection, rods and cones differ with respect to their G-protein α, β, and γ subunits, phosphodiesterase catalytic and inhibitory subunits, as well as the CNG-channel subunits. Exceptions do exist, such as recoverin, of which there is a single isoform shared by rods and cones). Functional divergence does result from subtle differences in rod/cone isoforms (and, to some degree, outer-segment morphology), giving rise to differences in signal amplification and signal kinetics, with rods showing much higher light sensitivity and cones showing better temporal resolution of light signals. As for M1- through M6-ipRGCs, we have found so far at least identical protein isoforms of the phototransduction components across them. Nonetheless, the percentage representations of the rhabdomeric vs. ciliary phototransduction pathways do vary across subtypes, likewise producing functional diversity. In principle, the expression levels of individual transduction proteins in each pathway can also vary across subtypes, producing different signal amplifications. For example, we know that the expression levels of melanopsin are different in different ipRGC subtypes, as indicated by melanopsin immunoreactivity or genetic labeling (see refs. 5–9). In short, although protein isoforms may be the same across subtypes, other factors can lead to diverse response properties. Ultimately, one needs a detailed knowledge of the brain target(s) that each ipRGC subtype projects to as well as the dynamic signaling properties of each specific neuronal circuit, before one can rationalize the proteomics based on function. Viewed as such, rods and cones are simpler in that there is so far no strong indication of major variations in corresponding phototransduction protein levels between rods and cones, or across cone subtypes (see, however, ref. 36).

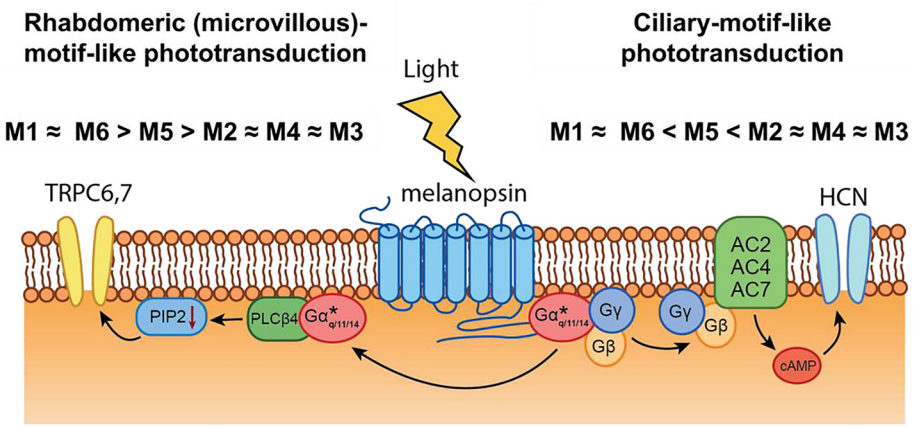

Fig. 10. Schematic diagram showing that the same PLCβ4/TRPC6,7 and cAMP/HCN phototransduction pathways coexist in M1- through M6-ipRGCs. M1≈M6>M5>M2≈M4≈M3 and M3≈M4≈M2>M5>M6≈M1 indicate the relative prevalence of each pathway in each ipRGC subtype based on integrated charge transfer. "*" indicates activated state. See text for details.

The level of protein-isoform redundancy in ipRGC phototransduction is surprisingly high, involving $G\alpha_q$, $G\alpha_{11}$, and $G\alpha_{14}$ in the PLCβ4/TRPC6,7 rhabdomeric pathway when compared to that in rods and cones or even other GPCR pathways. It is possible that such redundancy as found in ipRGCs has not been closely investigated in other signaling pathways as we have done in this work, because the gene-knockout approach is labor-intensive and very time-consuming. Another possibility is that such functional protein-isoform redundancy is only common to cells closer to their evolutionary ancestors. However, in the supposedly ancient jellyfish ciliary photoreceptors, which we have used in this work as a reference, such functional redundancy has not been reported (22). It is not just G protein α-subunits. Our work here suggests that at least as many as three ACs are involved in generating cAMP in the cAMP/HCN ciliary pathway. Nonetheless, the fact that more than one AC isoform is involved does not necessarily mean that they play equal roles in the signaling because they may have different affinities for Gβγ or have different catalytic rates. Finally, it is still unclear currently how many Gβγ isoforms are normally involved in signaling from $G_{q,11,14}$ to the ACs in ipRGCs.

Materials and Methods

All experiments were conducted according to the protocols approved by the Institutional Animal Care and Use Committee at Johns Hopkins University. Patch clamping recordings were carried out from ipRGCs in flat-mounted (ganglion-cell side up) mouse retinae isolated from the retinal pigment epithelium. Intravitreal injection of AAV virus, photouncaging of caged cAMP/cGMP compound, and immunohistochemistry were also used. See *SI Appendix, Materials and Methods* for experimental details.

Data, Materials, and Software Availability. All data in this study are available in the article and/or *SI Appendix*.

ACKNOWLEDGMENTS. We thank M. T. H. Do (Harvard Medical School) and C.-K. J. Chen (now at University of Texas College of Medicine San Antonio) for discussions at the 2023 FASEB Summer Meeting "The Biology and Chemistry of Vision". We thank T. Shelley for fabricating all customized devices, L. Ding and T. Du for mouse genotyping, and R. Li, Z. Chai, S. Li, and N. Gooya for comments and discussions. We also thank the two PNAS reviewers for very helpful comments on the manuscript. D. M. Berson (Brown University) kindly provided information about the *Cdh3-GFP* line (obtained from MMRRC), and P. C. Sternweis (UT Southwestern) kindly provided the strain resources for *Adcy7*$^{fl/fl}$ line, revived by the Core Animal Facility of Johns Hopkins University. *Adcy4*^{tm1Dgen} strain was from MMRRC. Finally, we thank the NINDS Multi-Photon Imaging Core at JHMI (P30 NS050274) for imaging help and data analysis. This work was supported by NIH Grant R01 EY014596 and by a Beckman-Argyros Vision Award to K.-W.Y.

Author affiliations: [a]Solomon H. Snyder Department of Neuroscience, Johns Hopkins University School of Medicine, Baltimore, MD 21205; and [b]Neuroscience Graduate Program, Johns Hopkins University School of Medicine, Baltimore, MD 21205

1. I. Provencio, G. Jiang, W. J. deGrip, W. P. Hayes, M. D. Rollag, Melanopsin: An opsin in melanophores, brain, and eye. *Proc. Natl. Acad. Sci. U.S.A.* **95**, 340–345 (1998).
2. D. M. Berson, F. A. Dunn, M. Takao, Phototransduction by retinal ganglion cells that set the circadian clock. *Science* **295**, 1070–1073 (2002).
3. S. Hattar, H. W. Liao, M. Takao, D. M. Berson, K.-W. Yau, Melanopsin-containing retinal ganglion cells: Architecture, projections, and intrinsic photosensitivity. *Science* **295**, 1065–1070 (2002).
4. M. T. H. Do, K.-W. Yau, Intrinsically photosensitive retinal ganglion cells. *Physiol. Rev.* **90**, 1547–1581 (2010).
5. T. M. Schmidt, S. K. Chen, S. Hattar, Intrinsically photosensitive retinal ganglion cells: Many subtypes, diverse functions. *Trends Neurosci.* **34**, 572–580 (2011).
6. M. T. H. Do, Melanopsin and the intrinsically photosensitive retinal ganglion cells: Biophysics to behavior. *Neuron* **104**, 205–226 (2019).
7. R. J. Lucas, A. E. Allen, N. Milosavljevic, R. Storchi, T. Woelders, Can we see with melanopsin? *Ann. Rev. Vis. Sci.* **6**, 453–468 (2020).
8. K. B. Sondereker, M. E. Stabio, J. M. Renna, Crosstalk: The diversity of melanopsin ganglion cell types has begun to challenge the canonical divide between image-forming and non-image-forming vision. *J. Comp. Neurol.* **528**, 2044–2067 (2020).
9. M. L. Aranda, T. M. Schmidt, Diversity of intrinsically photosensitive retinal ganglion cells: Circuits and functions. *Cell. Mol. Life Sci.* **78**, 889–907 (2021).
10. M. E. Stabio *et al.*, The M5 Cell: A color-opponent intrinsically photosensitive retinal ganglion cell. *Neuron* **97**, 150–163 (2018).
11. L. E. Quattrochi *et al.*, The M6 cell: A small-field bistratified photosensitive retinal ganglion cell. *J. Comp. Neurol.* **527**, 297–311 (2019).
12. K.-W. Yau, R. C. Hardie, Phototransduction motif and variations. *Cell* **139**, 246–264 (2009).
13. D. Arendt, Evolution of eyes and photoreceptor cell types. *Int. J. Dev. Biol.* **47**, 563–571 (2003).
14. T. D. Lamb, S. P. Collin, E. N. Pugh, Evolution of the vertebrate eye: Opsins, photoreceptors, retina and eye cup. *Nat. Rev. Neurosci.* **8**, 960–976 (2007).
15. D. M. Graham *et al.*, Melanopsin ganglion cells use a membrane-associated rhabdomeric phototransduction cascade. *J. Neurophysiol.* **99**, 2522–2532 (2008).
16. T. Xue *et al.*, Melanopsin signalling in mammalian iris and retina. *Nature* **479**, 67–73 (2011).
17. Z. Jiang, W. W. S. Yue, L. Chen, Y. Sheng, K.-W. Yau, Cyclic-nucleotide- and HCN-channel-mediated phototransduction in intrinsically photosensitive retinal ganglion cells. *Cell* **175**, 652–664 (2018).
18. L. Chen, G. Li, Z. Jiang, K.-W. Yau, Unusual phototransduction via cross-motif signaling from G_q to adenylyl cyclase in intrinsically photosensitive retinal ganglion cells. *Proc. Natl. Acad. Sci. U.S.A.* **120**, e2216599120 (2023).
19. J. Takasaki *et al.*, A novel $G\alpha_{q/11}$-selective inhibitor. *J. Biol. Chem.* **279**, 47438–47445 (2004).
20. P. A. Ferreira, W. L. Pak, Bovine phospholipase C highly homologous to the NorpA protein of *Drosophila* is expressed specifically in cones. *J. Biol. Chem.* **269**, 3129–3131 (1994).
21. Y. W. Peng *et al.*, Identification of components of a phosphoinositide signaling pathway in retinal rod outer segments. *Proc. Natl. Acad. Sci. U.S.A.* **94**, 1995–2000 (1997).
22. M. Koyanagi *et al.*, Jellyfish vision starts with cAMP signaling mediated by opsin-Gs cascade. *Proc. Natl. Acad. Sci. U.S.A.* **105**, 15576–15580 (2008).

23. T. Sonoda, S. K. Lee, L. Birnbaumer, T. M. Schmidt, Melanopsin phototransduction is repurposed by ipRGC subtypes to shape the function of distinct visual circuits. *Neuron* **99**, 754–767 (2018).
24. E. Contreras, A. P. Nobleman, P. R. Robinson, T. M. Schmidt, Melanopsin phototransduction: Beyond canonical cascades. *J. Exp. Biol.* **224**, jeb226522 (2021).
25. E. Contreras, T. Sonoda, L. Birnbaumer, T. M. Schmidt, Melanopsin activates divergent phototransduction pathways in ipRGC subtypes. *eLife* **12**, e80749 (2023). https://doi.org/10.1101/2022.06.12.495838.
26. M. T. H. Do *et al.*, Photon capture and signalling by melanopsin retinal ganglion cells. *Nature* **457**, 281–287 (2009).
27. C. W. Dessauer *et al.*, International union of basic and clinical pharmacology. CI. Structures and small molecule modulators of mammalian adenylyl cyclases. *Pharmacol. Rev.* **69**, 93–139 (2017).
28. D. M. F. Cooper, A. J. Crossthwaite, Higher-order organization and regulation of adenylyl cyclases. *Trends. Pharmacol. Sci.* **27**, 426–431 (2006).
29. F. C. Meotti, E. L. de Andrade, J. B. Calixto, TRP modulation by natural compounds. *Handb. Exp. Pharmacol.* **223**, 1177–1238 (2014).
30. L. I. Jiang, P. C. Sternweis, J. E. Wang, Zymosan activates protein kinase A via adenylyl cyclase VII to modulate innate immune responses during inflammation. *Mol. Immunol.* **54**, 14–22 (2013).
31. M. T. H. Do, Patch-clamp electrophysiological analysis of murine melanopsin neurons. *Circadian Clocks* **186**, 121–150 (2022).
32. M. J. V. Hook, D. M. Berson, Hyperpolarization-activated current (I_h) in ganglion-cell photoreceptors. *PLoS One* **5**, e15344 (2010).
33. S. C. Lee, A. T. Ishida, I_h without K_{ir} in adult rat retinal ganglion cells. *J. Neurophysiol.* **97**, 3790–3799 (2007).
34. A. Ludwig, X. Zong, M. I. Jeglitsch, F. Hofmann, M. Biel, A family of hyperpolarization activated mammalian cation channels. *Nature* **393**, 587–591 (1998).
35. R. Seifert *et al.*, Molecular characterization of a slowly gating human hyperpolarization-activated channel predominantly expressed in thalamus, heart, and testis. *Proc. Natl. Acad. Sci. U.S.A.* **96**, 9391–9396 (1999).
36. J. Baudin, J. Angueyra, R. Sinha, F. Rieke, S cone photoreceptors in the primate retina are functionally distinct from L and M comes. *eLife* **8**, e39166 (2019).